Journal of Volcanology and Geothermal Research 263 (2013) 122–131

Contents lists available at ScienceDirect

Journal of Volcanology and Geothermal Research

journal homepage: www.elsevier.com/locate/jvolgeores

Along-arc variations in lithospheric mantle compositions in Kamchatka, Russia: First trace element data on mantle xenoliths from the Klyuchevskoy Group volcanoes

D.A. Ionov [a,b,*], A. Bénard [a,b,1], P.Yu. Plechov [c], V.D. Shcherbakov [c]

[a] Université J. Monnet (member of PRES Université de Lyon), 42023 Saint Etienne, France
[b] Laboratoire "Magmas et Volcans" UMR6524-CNRS, 42023 Saint Etienne, France
[c] Moscow State University, Department of Geology, 119899 Moscow, Russia

ARTICLE INFO

Article history:
Received 23 February 2012
Accepted 31 December 2012
Available online 11 January 2013

Keywords:
Mantle xenolith
Harzburgite
Metasomatism
Trace elements
Subduction
Island arc

ABSTRACT

We provide results of a detailed study of the first peridotite xenoliths of proven mantle origin reported from Bezymyanny volcano in the Klyuchevskoy Group, northern Kamchatka arc. The xenoliths are coarse spinel harzburgites made up mainly of Mg-rich olivine as well as subhedral orthopyroxene (opx) and Cr-rich spinel, and also contain fine-grained interstitial pyroxenes, amphibole and feldspar. The samples are unique in preserving the evidence for both initial arc mantle substrate produced by high-degree melt extraction and subsequent enrichment events. We show that the textures, modal and major oxide compositions of the Bezymyanny xenoliths are generally similar to those of spinel harzburgite xenoliths from Avacha volcano in southern Kamchatka. However, coarse opx from the Bezymyanny harzburgites has higher abundances of light and medium rare earth elements and other highly incompatible elements than coarse opx from the Avacha harzburgites. We infer that (1) the sub-arc lithospheric mantle beneath both Avacha and Bezymyanny (and possibly between these volcanoes) consists predominantly of harzburgitic melting residues, which experienced metasomatism by slab-related fluids or low-fraction, fluid-rich melts and (2) the degrees of metasomatism are higher beneath Bezymyanny. By contrast, xenolith suites from Shiveluch and Kharchinsky volcanoes 50–100 km north of the Klyuchevskoy Group include abundant cumulates and products of reaction of mantle rocks with silicate melts at high melt/rock ratios. The high melt flux through the lithospheric mantle beneath Shiveluch and Kharchinsky may be related to the asthenospheric flow around the northern edge of the sinking Pacific plate; lateral propagation of fluids in the mantle wedge south of the plate edge may contribute to metasomatism in the mantle lithosphere beneath the Klyuchevskoy Group volcanoes.

1. Introduction

Fluids expelled from sinking oceanic lithosphere in subduction zones initiate island arc magmatism and contribute to global recycling of volatiles and fluid-mobile elements (van Keken, 2003; Churikova et al., 2007; Portnyagin et al., 2007). On the way to the surface, these fluids and related melts react with the mantle wedge and sub-arc mantle lithosphere and may be trapped. The upward migration of slab-related fluids and melts in the lithospheric mantle, initially composed of refractory melting residues, is responsible for a group of phenomena generally known as mantle metasomatism. These phenomena range from minor enrichments in incompatible trace elements of initially highly depleted rocks to precipitation in the refractory, Mg-rich peridotites of accessory grains or veins of amphibole (amph), phlogopite (phl), clinopyroxene (cpx), orthopyroxene (opx) and other minerals from fluids or fluid-rich, low-fraction melts (e.g. Maury et al., 1992; Ionov et al., 1997; Bedini and Bodinier, 1999; McInnes et al., 2001; Pearson et al., 2003). By comparison, reaction of mantle peridotites with percolating high-T silicate melts at high melt/rock ratios may either dissolve or precipitate olivine and pyroxenes to yield various hybrid and cumulate rocks (dunites, harzburgites, wehrlites, pyroxenites) with a broad range of Mg# [$Mg/(Mg+Fe)_{at}$] (e.g. Kelemen et al., 1992; Ionov et al., 2005b; Bryant et al., 2007; Tursack and Liang, 2012).

In general, mantle metasomatism must be more advanced and more widespread in arc sections with higher upward fluid flux. Hence, the fluid transfer to arc mantle can be assessed from degrees of metasomatism in the lithosphere while the compositions of the migrating fluids can be inferred from those of metasomatic products in mantle rocks, e.g. using partition coefficients. Of particular interest are studies of trace element compositions in common and most abundant mantle minerals (opx, cpx), which are likely to approach equilibrium with percolating fluids/melts, whereas the composition of accessory and vein minerals may provide information only on small fluid portions trapped in fractures and interstitial pockets.

The degrees of metasomatism and the nature of fluids in sub-arc mantle may be directly constrained from studies of mantle fragments

* Corresponding author at: Université J. Monnet (member of PRES Université de Lyon), 42023 Saint Etienne, France. Tel.: +33 477481512.
E-mail address: dmitri.ionov@univ-st-etienne.fr (D.A. Ionov).
[1] Present address: Research School of Earth Sciences, The Australian National University, Canberra, ACT 0200, Australia.

0377-0273/$ – see front matter © 2013 Elsevier B.V. All rights reserved.
http://dx.doi.org/10.1016/j.jvolgeores.2012.12.022

(xenoliths) carried to the surface by magmas in modern arcs. A difficulty with this approach is that such xenoliths are rare in arc volcanic rocks worldwide. One of very few exceptions is the eastern seaboard of the Kamchatka peninsula in NE Russia where peridotite mantle xenoliths were recently reported from Avacha and Shiveluch (Sheveluch) volcanoes (Bryant et al., 2007; Ishimaru et al., 2007; Ionov, 2010). The Avacha and Shiveluch xenolith suites show some important textural and chemical differences, which may be due either to distinct lithospheric mantle compositions on a regional scale (the two sites are ~400 km apart along the volcanic front, Fig. 1) or to widespread mantle–melt interaction for the Shiveluch suite (Bryant et al., 2007), which may only take place in the regions of high upward melt flux through the mantle as well as in the vicinity of melt conduits and chambers. Data on xenoliths from other Kamchatka volcanoes are essential for further insights into the mantle composition in the arc.

We report petrographic, major and trace element data on lithospheric mantle xenoliths from Bezymianny volcano located between Avacha and Shiveluch. This paper provides first trace element data on the most common minerals in sub-arc mantle beneath the Klyuchevskoy Group of volcanoes, one of the most productive among currently active volcanic sites worldwide, as well for the mantle beneath the northern Kamchatka in general. The data are used here to shed more light on melting and metasomatism in the mantle beneath the Kamchatka arc and their relation to tectonic settings. We show, in particular, that the lithospheric mantle beneath the Klyuchevskoy Group appears to consist mainly of the same rock type (refractory spinel harzburgite) as beneath Avacha, but is more metasomatized, possibly because of a location in the vicinity of a slab edge or slab anomaly and, hence, higher fluid flux in the mantle (e.g. Davaille and Lees, 2004).

2. Geological context and samples

Bezymianny is an andesitic volcano (55°58′ N, 160° 36′ E) on the southern flank of the Klyuchevskoy Group of volcanoes situated in the central segment of the Kamchatka peninsula formed from accreted Mesozoic and Tertiary oceanic and island arc terrains with crustal thickness

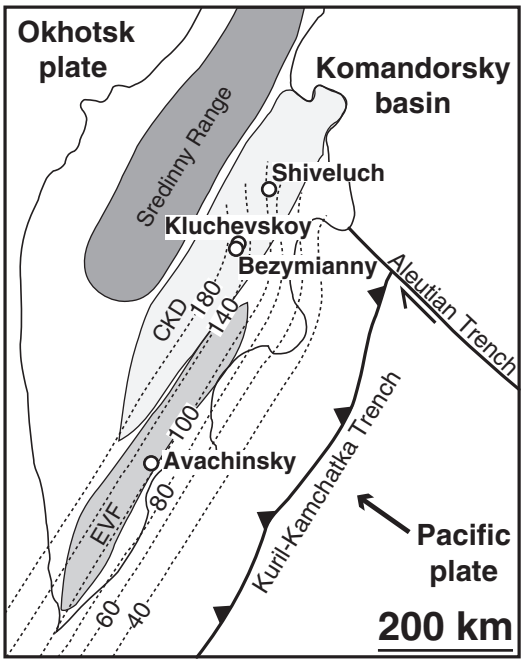

Fig. 1. Location map for Bezymianny and other Kamchatka volcanoes and an outline of regional tectonic setting. Continuous bold lines show position of subduction trenches in the western Pacific; dotted lines with numbers show the depth to the top of the slab in km. EVF, eastern volcanic front; CKD, central Kamchatka depression. Modified after Gorbatov et al. (1999) and Portnyagin et al. (2007).

of 30–40 km (Konstantinovskaya, 2001). The Klyuchevskoy Group is a continuation of the Eastern Volcanic Front (EVF) to north of Kamchatka facing the junction between the Aleutian and Kamchatka subduction systems (Fig. 1). Geophysical and geochemical data indicate asthenospheric mantle flow around the edge of the Pacific slab in the region (e.g. Davaille and Lees, 2004). This unique tectonic setting has been linked to the high productivity and a broad compositional range of the Klyuchevskoy Group and Shiveluch volcanoes (Yogodzinski et al., 2001). Recent seismic data outline a complex lithospheric structure in the Klyuchevskoy area including: (1) an unusual planar, sharply bounded, dipping seismic feature in the mantle wedge ~100 km deep interpreted as the source of melts erupting at the Klyuchevskoy Group (Nikulin et al., 2010), (2) a large magma chamber (or a series of small chambers) below 25–30 km, i.e. near the bottom of the crust, (3) intermediate magma storage volumes at 8–13 km and (4) a shallow chamber beneath Klyuchevskoy (Koulakov et al., 2011).

No peridotite xenoliths of undisputed lithospheric mantle origin have as yet been reported from the Klyuchevskoy Group in the international literature, even though olivine-rich inclusions in Klyuchevskoy lavas were first reported in Russian several decades ago (Piip, 1956). Like for most other arc volcanoes, this may be related to the existence of multiple magma storage levels where mantle-derived magmas pool on the way to the surface; as a result the dense mantle xenoliths settle to the bottom of magma chambers and are buried and/or assimilated. October 2007 eruption of Bezymianny brought up to the surface small peridotite fragments representing lithospheric mantle (Shcherbakov and Plechov, 2010). They are enclosed in rounded porphyric plagioclase–opx–cpx enclaves in lava associated with a pyroclastic flow. Two xenoliths reported here (CK09-7c; CK09-20) were sawn to produce ~100 μm thick polished sections for micro-beam analyses and petrographic inspection (Fig. 2). More information on the locality, host volcanic rocks (Dorendorf et al., 2000; Eichelberger et al., 2007; Portnyagin et al., 2007) as well as preliminary data on petrography and major element composition of the xenoliths were reported recently (Shcherbakov and Plechov, 2010; Shcherbakov et al., 2011).

The Bezymianny xenoliths are considered here mainly in comparison with data on abundant, large (>5–10 cm), unaltered spinel harzburgite xenoliths from Avacha, which have been extensively studied (Ishimaru et al., 2007; Weyer and Ionov, 2007; Ionov and Seitz, 2008; Halama et al., 2009; Ionov, 2010; Soustelle et al., 2010; Bénard et al., 2011; Hopp and Ionov, 2011; Ionov et al., 2011; Ishimaru and Arai, 2011; Pogge von Strandmann et al., 2011; Bénard and Ionov, 2012). The Avacha strato-volcano within the EVF in southern Kamchatka (Fig. 1) erupts mainly basaltic and low-K andesites as ash-falls and pyroclastic flows. The ~80 Ma Pacific plate is subducted beneath the southern Kamchatka arc at a rate of 7–9 cm/a dipping at 55°. Depth to the slab is ~120 km, slab thickness is ~70 km. Seismic data indicate a crustal thickness of ~37 km; low P-wave velocities beneath the Moho were interpreted as indicative of the presence of melt (Gorbatov et al., 1999; Manea et al., 2005).

3. Analytical methods

Major element analyses of minerals and back-scattered electron (BSE) images were mainly obtained by wavelength-dispersive (WD) electron probe micro-analysis (EPMA) on a CAMECA SX100 instrument at the Laboratoire Magmas et Volcans (LMV, Clermont-Ferrand, France) with accelerating voltage of 15 kV and sample current of 15 nA for olivine, pyroxenes and amphibole, and 4 nA for feldspar and glass; defocused electron beam was used to limit alkali loss in the latter. Counting times were 5–10 s for background and 10–20 s for peaks. Matrix effects were corrected using Phi (r) z Peak Sight© software from CAMECA™. Typical standard deviations (3 σ) are 0.1–0.3 wt.% for Si, Ca, Na and Al and 0.03–0.1 wt.% for Fe, Cr, K, Ti, Mg and Mn. Some data and images were obtained with energy-dispersive spectroscopy (EDS) on a JEOL JSM-6480LV with an X-ray INCA-Energy-350

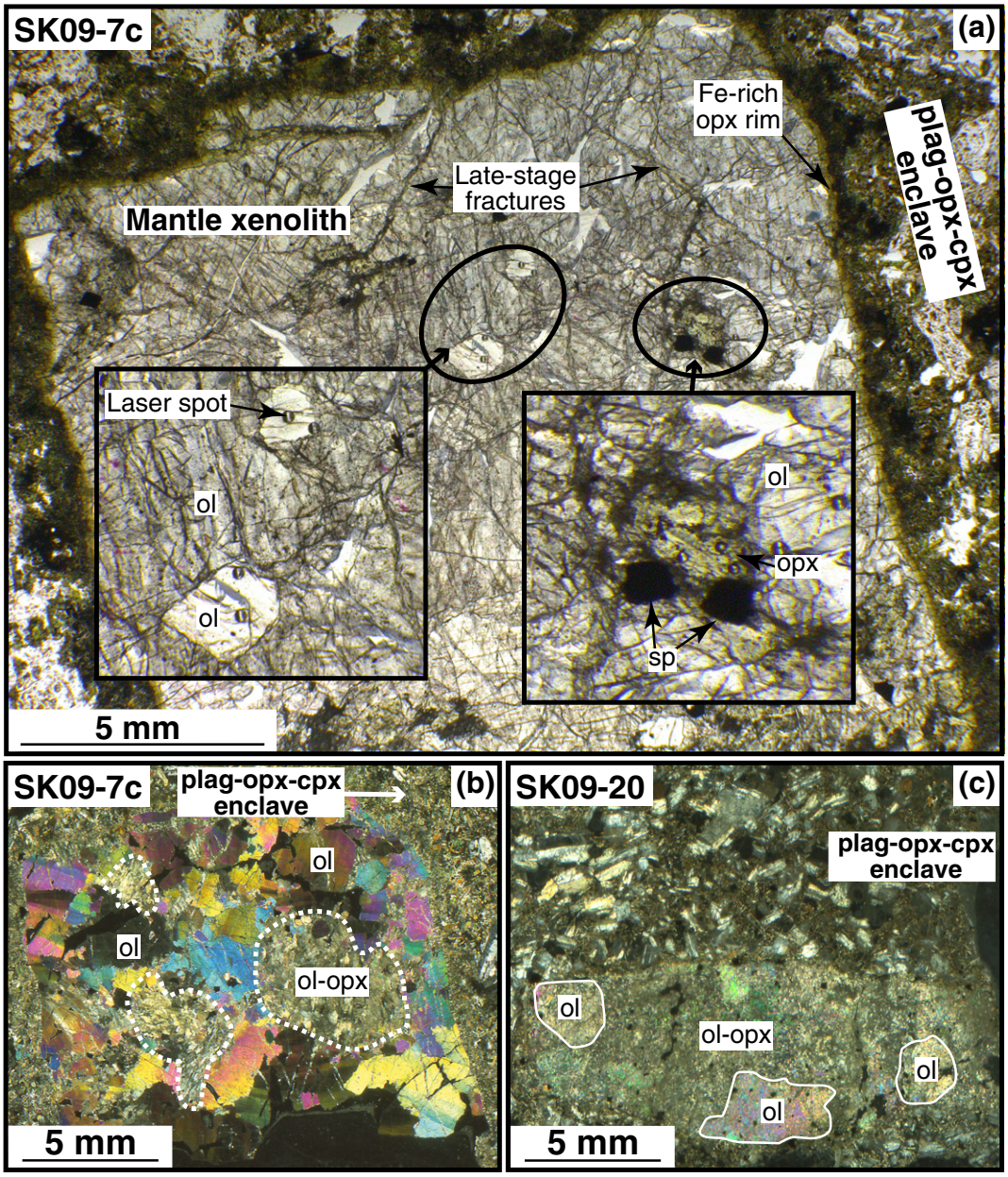

Fig. 2. (a–c). Photomicrographs of peridotite xenoliths from Bezymianny in transmitted plane-polarized (a) and cross-polarized (b, c) light. (a) Xenolith CK09-7c has a reaction rim of brown, fine-grained, Fe-rich orthopyroxene (opx) and is enclosed in a porphyroclastic aggregate of plagioclase (plag), clinopyroxene (cpx) and opx. The insets show enlarged areas including clear olivine (ol) grains with laser ablation pits (left) and 1st-generation opx and spinel (sp) (right). (b) A section of xenolith CK09-7c cut close to and parallel to the contact with host magma. Late-stage, fine-grained aggregates (outlined with white dashed lines) are common next to the contact but are rare in the section plane in the middle of the xenolith (see (a)). (c) Fine-grained xenolith SKO9-20 recrystallized as a result of reaction with host magma. Relics of coarse olivine are outlined with white lines.

Micro-analyser and on a scanning electron microscope at the Moscow State University (MSU).

Trace elements were measured by Laser-Ablation Inductively Coupled Plasma Mass-Spectrometry (LA-ICPMS) at the LMV on an Agilent 7500 coupled with an UV (193 nm) Excimer Resonetics M-50E laser system in helium flux. Ablation was done at 1–5 Hz, ~12 $J \cdot cm^{-2}$ and beam size of 100 μm. Calibration was done with the NIST 612 glass and Si as internal standard. Reference sample BCR-2g was measured for quality control, with relative standard deviation (1 σ) of 0.4–3% at ppm abundances. The full analytical dataset is available as Online supplement 1.

4. Petrography and major element composition of minerals

At the contact with the host rocks, the xenoliths develop dark-brown, fine-grained reaction rims (Fig. 2). The rims consist mainly of Fe-rich opx (Table 1); they are 0.1–0.3 mm thick if they replace coarse opx and olivine but may be thicker and form "inlets" when in contact with fine-grained, late-stage materials (Online supplement 2). The xenoliths also contain crosscutting or interstitial veins; some of them are connected to the xenolith rims via fractures (Fig. 2a). The harzburgite xenoliths are not hosted directly by lavas but occur in essentially crystalline, doleritic "enclaves" 5–30 cm in size consisting of predominant porphyric, zoned plagioclase and smaller grains of opx, cpx and opaque minerals (Fig. 2). These enclaves appear to have formed by crystallization of mantle-derived magmas and crystal accumulation in intermediate magma chambers (Shcherbakov and Plechov, 2010); the magmas carried peridotite xenoliths, which reacted with the magmas and were trapped by their crystallization products. Later intrusions of fresh batches of magma fragmented the early cumulates and brought them as "enclaves" to the surface together with enclosed mantle xenoliths that have not been consumed by the magma.

Table 1
Representative EPMA (wt.%) of phases in Bezymianny xenolith CK09-7c, its opx rim and host.

Rock type	M.X.	M.X.	M.X.	M.X.	M.X.	M.X.	M.X.	M.X.	M.X.	M.X.
Mineral	ol 1 core	ol 1 rim	ol 2 core	ol 2 rim	opx 1 core	opx 1 rim	cpx 2 core	cpx 2 rim	sp 2 core	sp 2 rim
SiO_2	41.75	41.82	40.70	40.53	56.92	57.73	53.55	54.06	0.02	0.05
TiO_2	b.d.	b.d.	b.d.	b.d.	b.d.	0.01	0.03	0.01	0.25	0.38
Al_2O_3	b.d.	b.d.	b.d.	b.d.	2.26	1.48	1.14	1.86	22.14	23.29
Cr_2O_3	b.d.	b.d.	b.d.	b.d.	0.47	0.10	0.07	0.32	31.75	34.95
FeO	9.07	8.89	9.32	9.35	6.34	6.07	2.80	3.13	30.80	25.29
MnO	0.11	0.17	0.08	0.09	0.10	0.15	0.12	0.18	0.25	0.26
MgO	49.16	49.48	50.07	50.44	34.80	34.83	18.09	17.56	12.70	13.15
CaO	0.04	0.05	0.05	0.07	0.14	0.40	23.91	23.22	b.d.	b.d.
Na_2O	b.d.	b.d.	b.d.	b.d.	b.d.	0.01	0.18	0.24	b.d.	b.d.
K_2O	b.d.	b.d.	b.d.	b.d.	b.d.	b.d.	b.d.	b.d.	b.d.	b.d.
NiO	0.40	0.37	0.49	0.39	0.05	0.11	0.12	0.10	0.39	0.22
Total	100.56	100.81	100.75	100.95	101.07	100.92	100.03	100.67	98.38	97.67
Mg#	0.906	0.908	0.905	0.906	0.907	0.911	0.920	0.909	0.424	0.481
Cr#	–	–	–	–	0.122	0.044	0.038	0.102	0.490	0.502

Rock type	M.X.	M.X.	M.X.	M.X.	M.X.	M.X.	M.X.	M.X.	M.X.	M.X.
Mineral	ol relic core	ol 3 core	ol 3 rim	opx 3 core	cpx 3 core	sp 3 core	amph 3 core	amph 3 rim	plag 3	plag 3
SiO_2	41.19	41.20	40.87	56.62	52.59	0.10	44.02	44.36	48.49	58.00
TiO_2	b.d.	b.d.	b.d.	0.09	0.24	0.19	0.46	0.56	0.02	0.02
Al_2O_3	b.d.	b.d.	b.d.	2.38	3.84	22.72	13.54	13.28	33.09	26.20
Cr_2O_3	b.d.	b.d.	b.d.	0.06	1.28	36.55	0.95	0.86	–	–
FeO	9.44	9.35	10.68	6.90	3.27	24.41	5.20	5.20	0.60	0.61
MnO	0.16	0.15	0.19	0.21	0.07	0.21	0.01	0.07	0.08	0.00
MgO	49.52	48.69	48.04	33.70	16.49	12.80	18.08	17.75	0.07	0.09
CaO	0.10	0.13	0.20	0.74	22.89	b.d.	11.54	11.99	15.93	8.42
Na_2O	b.d.	b.d.	b.d.	0.06	0.27	b.d.	2.66	2.61	2.12	5.87
K_2O	b.d.	b.d.	b.d.	b.d.	b.d.	b.d.	0.56	0.55	0.22	1.18
NiO	0.32	0.40	0.47	0.10	0.06	0.27	0.20	0.20	–	–
Total	100.79	100.04	100.50	100.85	101.01	97.50	97.21	97.43	100.75	100.68
Mg#	0.903	0.903	0.889	0.897	0.900	0.483	0.861	0.859	–	–
Cr#	–	–	–	0.016	0.182	0.519	0.045	0.041	–	–

Rock type	RIM	RIM	RIM	RIM	H.E.	H.E.	H.E.	H.E.	H.E.	H.E.
Mineral and glass	opx	opx	opx	opx	cpx core	cpx rim	plag core	plag core	plag rim	Glass
SiO_2	56.14	54.99	54.20	55.07	51.76	53.23	50.40	50.47	53.94	73.41
TiO_2	0.16	0.11	0.10	0.25	0.50	0.35	0.00	0.05	0.00	0.93
Al_2O_3	1.52	1.51	1.69	1.57	2.25	1.23	31.20	31.29	28.70	12.56
Cr_2O_3	0.00	0.02	0.07	0.09	0.03	0.03	0.04	0.00	–	0.01
FeO	11.83	14.65	17.11	17.11	9.82	8.86	0.53	0.40	0.54	2.62
MnO	0.47	0.50	0.55	0.63	0.41	0.39	0.00	0.02	0.03	0.07
MgO	30.31	28.09	25.88	25.85	14.14	15.17	0.05	0.04	0.11	0.46
CaO	0.68	0.76	0.85	1.19	20.73	21.18	14.26	15.00	11.99	1.48
Na_2O	0.01	0.02	0.04	0.00	0.38	0.25	3.17	3.16	4.68	2.33
K_2O	b.d.	b.d.	b.d.	b.d.	b.d.	b.d.	0.12	0.13	0.52	3.17
NiO	0.09	0.05	0.03	0.03	0.04	0.01	b.d.	0.03	–	b.d.
Total	101.22	100.72	100.53	101.78	100.06	100.71	99.76	100.59	100.57	97.04
Mg#	0.820	0.774	0.729	0.729	0.720	0.753	–	–	–	0.239
Cr#	–	0.009	0.028	0.037	0.009	0.016	–	–	–	–

Ol, olivine; opx, orthopyroxene; cpx, clinopyroxene; sp, spinel; ol rel., olivine relic in opx 1; amph, amphibole; plag, plagioclase; M.X., mantle xenolith; RIM, Fe-rich opx rim at xenolith edges; H.E., host enclave; b.d., below detection limit; $Mg\# = Mg/(Mg + Fe)_{at}$; $Cr\# = Cr/(Cr + Al)_{at}$.

Among the samples in this study, xenolith CK09-7c has been least affected by interaction with host magma; its central part appears to have largely preserved the microstructures, modal and chemical composition of its mantle source region. It is a medium- to coarse-grained spinel harzburgite containing three structural groups of minerals. The principal group (1st generation) mainly consists of coarse (1–5 mm) olivine (80–90% of the rock), which contains abundant cracks, trails of fluid inclusions and shows sub-grains and undulose extinction (Fig. 2a–b), i.e. evidence for strain and plastic deformation (e.g. Soustelle et al., 2010). Less abundant are smaller (0.3–1 mm), subhedral grains of opx, spinel and clear, less strained olivine (Figs. 2a and 3a). The second structural group is interstitial or replaces the rims of 1st-generation mineral grains. It consists of fine-grained (0.1–0.3 mm) domains of intergrown opx, olivine and minor cpx as well as subhedral, spongy Cr-spinel with abundant silicate inclusions and vesicles (Fig. 3a–b) (cf. Ionov et al., 2011). The 3rd-generation materials (very fine-grained olivine, cpx, amphibole and feldspar) are least common; they fill cracks, overgrow corroded rims of spinel, form pockets replacing other minerals (Fig. 3b–d and Online supplement 2). Of particular interest is the occurrence of Na–Ca feldspar (Fig. 3c and Online supplement 3), which is rare in mantle xenoliths worldwide but was previously reported in xenolith suites at the Pacific margin of Eurasia (Ionov et al., 1999).

Representative EPMA for minerals of different generations in xenolith CK09-7c and its host enclave are given in Table 1; full data set is provided in Online supplement 1. The cores of olivine grains in xenolith CK09-7c have Mg# [$Mg/(Mg + Fe)_{at}$] (0.90–0.91), high NiO (~0.4 wt.%) (Fig. 4a) and low CaO (<0.1 wt.%). 1st-generation

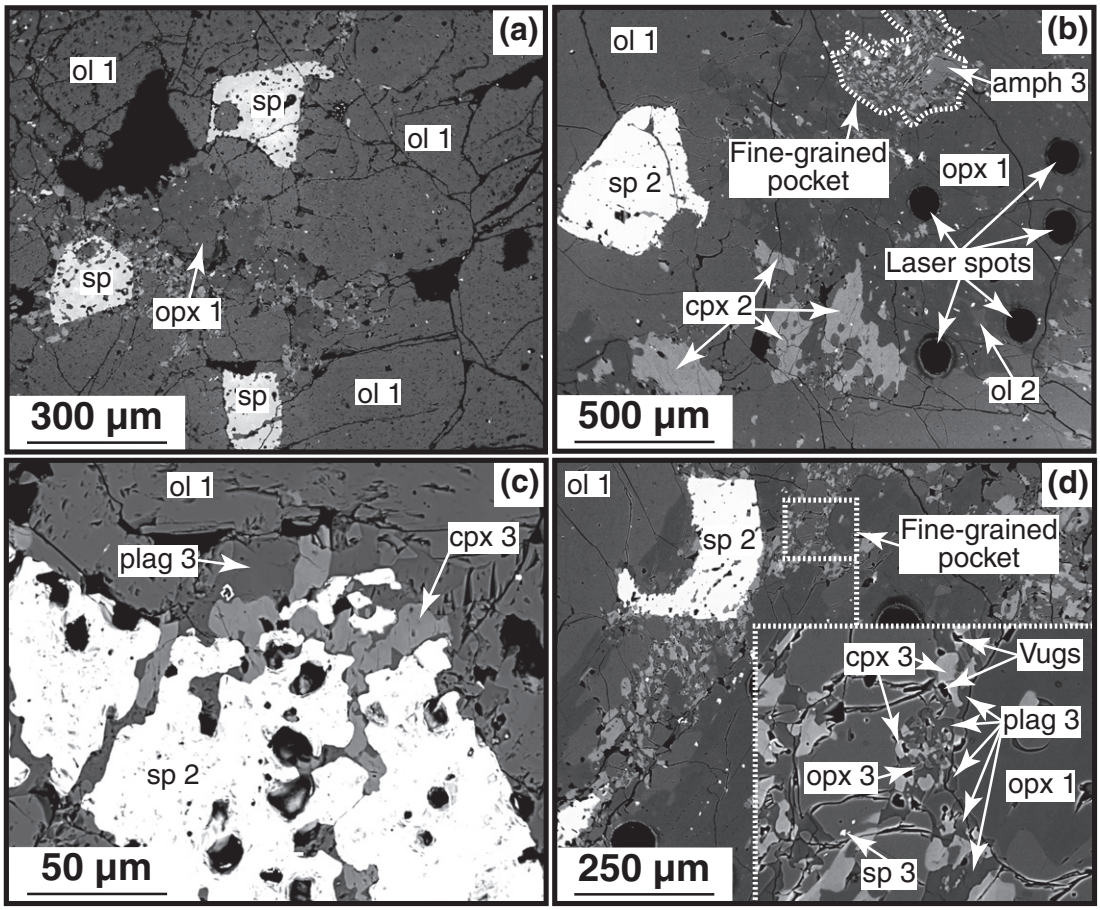

Fig. 3. (a–d). Back-scattered electron (BSE) images of Bezymianny xenolith CK09-7c. (a) Coarse, 1st-generation olivine (ol 1) and orthopyroxene (opx 1), and spinel (sp) (b) 1st-generation opx grain with laser ablation pits, 2nd-generation olivine (ol 2) and cpx (cpx 2) near opx rims, spongy spinel (sp 2) and 3rd-generation fine-grained pockets containing amphibole (amph 3). (c) Rims of a 2nd-generation spongy spinel grain replaced with an aggregate of 3rd-generation cpx and plagioclase (plag 3). (d) Structure of 3rd-generation fine-grained pockets consisting of intergrown late-stage opx, cpx and feldspar with empty vesicles (vugs).

opx has Mg# 0.90–0.92 and contains 1.8–2.5 wt.% Al_2O_3, 0.2–0.6 wt.% Cr_2O_3 and 0.1–0.4 wt.% CaO (Fig. 4b–c). Spinel cores have Mg# 0.35–0.42 and Cr# [$Cr/(Cr+Al)_{at}$] 0.5. The 2nd-generation cpx is rich in Ca, low in Na (≤0.5 wt.% Na_2O) and shows a broad range of Al_2O_3 (1–3 wt.%) and Cr_2O_3 (Fig. 4d). Rims of coarse olivine and opx may have lower Mg# and NiO than the cores while the opx rims have lower Al_2O_3 and Cr_2O_3 (Fig. 4). 3rd-generation amphibole has relatively low Mg# (0.86) while pyroxenes have more variable Al_2O_3 and Cr_2O_3 than 1st- and 2nd-generation minerals (Fig. 4b–d). The feldspar contains 2–6 wt.% Na_2O and ≤1.2 wt.% K_2O. Overall, the 1st-, 2nd- and 3rd-generation minerals are considered here as, respectively: (1) residues of melt extraction, (2) products of mantle metasomatism and exsolution from high-T opx on cooling, and (3) interaction of the xenoliths with host magma.

The cpx–opx and Ca–opx thermometry (Brey and Köhler, 1990) for 1st- and 2nd-generation minerals yields very low equilibration temperatures (T) of 800–900 °C (assuming pressures of 1.2–1.5 GPa). These values are below the experimental calibration range for the methods and hence approximate for individual opx grains or opx–cpx pairs, but taken together they clearly indicate that the Bezymianny xenoliths come from a very cold, hence shallow, mantle domain, possibly just under the Moho. Oxygen fugacity (fO_2) was calculated using the olivine–opx–spinel oxybarometer of Wood et al. (1990), with Fe^{3+}/Fe ratios in spinel estimated based on stoichiometry. The fO_2 values, expressed as log units relative to the fayalite–magnetite–quartz oxygen buffer (FMQ), range from +1.5 to +3 (see also Shcherbakov and Plechov, 2010). These fO_2 estimates have low precision compared to those based on Fe^{3+}/Fe in spinel obtained by Mössbauer spectroscopy or by EPMA using spinel standards with known Fe^{3+}/Fe (e.g. Wood et al., 1990; Bryant et al., 2007), yet they outline very high fO_2 typical of arc mantle worldwide (Ionov and Wood, 1992; Brandon and Draper, 1996; Parkinson and Arculus, 1999; McInnes et al., 2001; Parkinson et al., 2003; Ionov, 2010).

Xenolith CK09-20 (Fig. 2c) is made up of fine-grained olivine ($Fo_{85–88}$) surrounding relics of fractured, coarse olivine grains (Fig. 2c), opx (Mg# 0.86–0.89) and spinel (Cr# 0.6–0.7, Mg# 0.42–0.47) and contains accessory amphibole and anhydrite (Online supplement 1). We interpret these structures, mineral assemblages and compositions as products of recrystallization during xenolith–magma interaction.

5. Trace elements in minerals

Amphibole and cpx in the Bezymianny xenoliths, i.e. main carrier phases of incompatible trace elements in peridotites, are too small for LA-ICPMS analyses. Moreover, these minerals are 2nd- and 3rd-generation phases deposited by late-stage processes in the rocks, that may have taken place shortly before or during the transport of the xenoliths to the surface and could be affected by fluid/melt intrusion during xenolith–magma interaction. Our trace element data were mainly obtained on cores of 1st-generation opx grains from sample CK09-7c, which are more likely to keep record of more ancient mantle events, unrelated to their exhumation by volcanic activity. These data are examined here mainly in comparison with published LA-ICPMS data on coarse opx from Avacha spinel harzburgites (Ionov, 2010).

Representative trace element analyses of opx and olivine are given in Table 2; a complete set of LA-ICPMS data is provided in Online

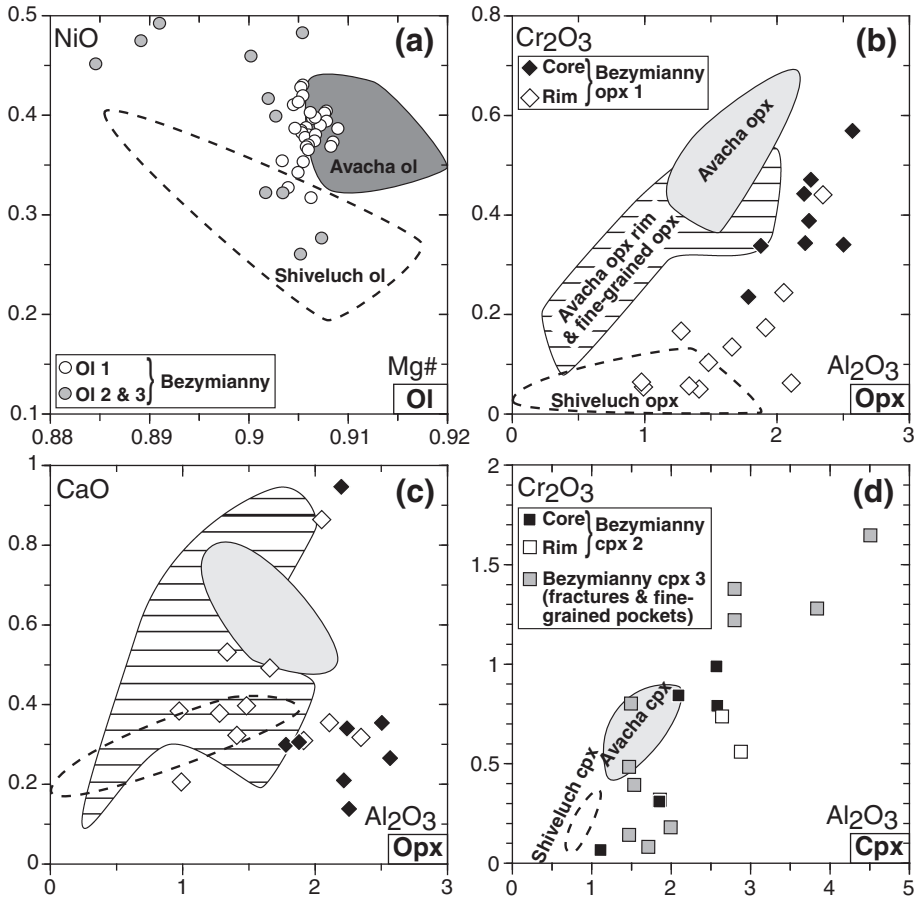

Fig. 4. (a–d). Co-variation plots of major oxides (wt.%) and Mg# [$Mg/(Mg+Fe)_{at}$] in minerals from xenolith CK09-7c. (a) Mg# vs. NiO in olivine, (b) Al_2O_3 vs. Cr_2O_3 in opx, (c) Al_2O_3 vs. CaO in opx, and (d) Al_2O_3 vs. Cr_2O_3 in cpx. Also shown are fields for minerals in harzburgite xenoliths from Avacha after Ionov (2010) (gray fields for cores of coarse grains; fields with horizontal lines are for rim and 2nd-generation opx) and for peridotite xenoliths from Shiveluch after Bryant et al. (2007) (dashed lines).

supplement 1. Primitive mantle-normalized patterns of rare earth elements (REE) and yttrium for the opx and olivine from xenolith CK09-7c are shown in Fig. 5a. The opx are low in heavy REE ($HREE_N$ ~0.02–0.3 where "N" shows abundances normalized to primitive mantle values after McDonough and Sun (1995)) compared to opx from fertile mantle spinel peridotites (e.g. Ionov et al., 2005a). The $HREE_N$ decrease from Lu to Ho, the medium REE_N ($MREE_N$) are nearly constant while the light REE_N ($LREE_N$) increase continuously from Sm to Ce or La; as a result the REE patterns are spoon- or U-shaped (Fig. 5a), which is common in cryptically metasomatized peridotites enriched in highly incompatible elements (Bedini and Bodinier, 1999; Pearson et al., 2003). The opx are also enriched in Th and U (but not in Nb) relative to LREE and in Ti, Zr and Hf relative to MREE (Fig. 5b). Importantly, the abundances of MREE–LREE and other highly incompatible elements in the Bezymianny opx are systematically higher than for coarse opx from Avacha peridotite xenoliths (Ionov, 2010); the latter show no spoon-shaped REE patterns but rather define a continuous decrease from $HREE_N$ to MREE–$LREE_N$ (Fig. 5). The HREE-Y patterns of olivine from the Bezymianny xenoliths are similar to those of opx but the concentrations are much lower (Fig. 5a); the abundances of other trace elements are below detection limits. Like for the opx, the REE abundances in the olivine are higher than in olivine from Avacha xenoliths (Fig. 5a).

6. The origin and evolution of arc mantle beneath Bezymianny

The combined petrographic, major and trace element data on the xenoliths in this study outline a three-stage history for the evolution of the lithospheric mantle beneath Bezymianny.

(1) Initially, a refractory harzburgitic protolith was formed by high-degree melt extraction. The absence of coarse, euhedral (1st-generation) cpx in the xenoliths indicates that the cpx was completely consumed by melting (experimental data require 23% anhydrous batch melting, or somewhat lower degrees of fractional melting, to remove cpx at 1 GPa (Herzberg, 2004)). Furthermore, the relatively low abundances of 1st-generation opx (Fig. 2a) suggest that the melting could continue further, possibly to 30–45%, to consume much of the initially present opx. The high melt extraction degrees are more likely during hydrous melting in subduction environments than beneath mid-ocean ridges (Parkinson and Pearce, 1998; Walter, 2003), but the melting conditions and degrees are hard to constrain precisely because experimental data for high-degree hydrous melting are scarce. Turner et al. (2007) argued that the melting processes beneath Klyuchevskoy and Bezymianny are complex, influenced by both fluid addition from the subducting plate and decompression beneath the Central Kamchatka Depression. The refractory residues were subsequently incorporated into the lithosphere where they cooled down and experienced deformation, which produced kink-banding in coarse olivine similar to that described for xenoliths from Avacha (Soustelle et al., 2010).

(2) The melting residues initially contained high-T opx relatively rich in Ca and Al. While the residues cooled down to 800–900 °C, these components exsolved from the residual, coarse opx to form interstitial, 2nd-generation pyroxenes at the rims of coarse opx grains. At this or at a later stage of the lithospheric mantle evolution, the residues experienced cryptic metasomatism, in particular the opx was enriched in incompatible trace elements (Fig. 5),

Table 2
Representative LA-ICPMS analyses of opx and olivine in Bezymianny xenolith CK09-7c and averages for reference sample BCR-2g.

Mineral	opx 1 core	opx 1 rim	opx 1 core	opx 1 rim	opx 1 core	opx 1 core	opx 1 rim	BCR-2 (Av. 3)	% Std. Dev.
CaO (EPMA)	0.34	0.40	–	0.94	0.35	0.38	–	–	–
CaO (LA-ICPMS)	0.42	0.51	0.41	0.90	0.39	0.51	0.43	7.27	1.2
Ti	104	83	70	85	71	82	125	13,599	1.9
V	83	68	60	76	68	81	41	435	0.5
Co	66	59	57	52	59	65	60	39	0.8
Ni	1022	645	885	744	741	1010	729	12	1.5
Zn	95	53	52	45	48	88	49	150	2.1
Ga	3.5	2.5	2.1	2.5	2.2	3.1	2.4	23.2	1.3
Sr	0.775	2.540	0.554	7.410	1.664	1.766	1.984	340	0.4
Y	0.242	0.252	0.113	0.219	0.181	0.260	0.332	30.3	1.4
Zr	1.065	2.248	1.019	2.390	1.515	1.250	2.208	169.8	1.7
Nb	0.083	0.058	0.034	0.058	0.050	0.066	0.041	12.27	0.5
Ba	2.680	1.840	1.265	3.860	1.283	1.790	2.650	714.69	1.2
La	0.0689	0.1631	0.0687	0.2910	0.1058	0.0930	0.1106	24.44	0.8
Ce	0.1950	0.4170	0.1590	0.5340	0.2740	0.2640	0.2490	54.26	1.9
Pr	0.0176	0.0400	0.0158	0.0457	0.0280	0.0312	0.0256	6.48	0.9
Nd	0.0691	0.1430	0.0529	0.1120	0.0712	0.1150	0.0970	28.58	0.7
Sm	0.0190	0.0271	b.d.	b.d.	0.0262	0.0171	0.0221	6.58	0.9
Eu	0.0048	0.0083	0.0038	0.0052	0.0053	0.0076	0.0068	1.94	2.1
Gd	0.0224	0.0307	b.d.	0.0157	0.0150	0.0235	0.0265	6.23	0.6
Tb	0.0034	0.0055	0.0025	0.0030	0.0035	0.0049	0.0055	0.92	0.7
Dy	0.038	0.032	0.020	0.025	0.025	0.036	0.046	6.09	0.5
Ho	0.0096	0.0085	0.0050	0.0083	0.0076	0.0097	0.0125	1.21	1.2
Er	0.041	0.036	0.018	0.031	0.030	0.037	0.039	3.43	1.5
Tm	0.009	0.007	0.006	0.006	0.006	0.009	0.009	0.48	2.7
Yb	0.068	0.080	0.053	0.065	0.060	0.086	0.081	3.28	0.4
Lu	0.018	0.015	0.011	0.015	0.010	0.014	0.018	0.47	1.8
Hf	0.025	0.026	0.013	0.028	0.0085	0.022	0.0523	4.38	0.7
Pb	0.152	0.065	0.076	0.115	0.050	0.034	0.035	11.16	2.4
Th	0.0240	0.0600	0.0251	0.0706	0.0322	0.0288	0.0615	5.670	1.3
U	0.0154	0.0201	0.0104	0.0197	0.0233	0.0094	0.0165	1.817	3.2
Mineral	ol 1 core	ol 1 core	ol 1 core	ol 1 rim	ol 1 rim	ol 1 rim	ol 1 rim	BCR-2 (Av. 3)	% Std. Dev.
CaO (EPMA)	0.05	–	–	0.05	–	–	–	–	–
CaO (LA-ICPMS)	0.03	0.12	0.03	0.04	0.04	0.04	0.04	7.27	1.2
Ti	5.6	19.3	5.5	5.7	3.6	5.1	5.0	13,599	1.9
V	1.5	7.7	1.2	4.5	3.0	1.5	1.5	435	0.5
Co	148	147	151	149	156	151	153	39	0.8
Zn	60	66	59	63	70	58	59	150	2.1
Y	0.014	0.073	0.009	0.011	0.010	0.010	0.005	169.8	1.7
Yb	0.0234	0.0232	0.0143	0.0063	0.0070	0.0080	0.0139	3.28	0.4
Lu	0.0036	0.0077	0.0029	b.d.	b.d.	0.0035	0.0020	0.47	1.8

Ol, olivine; opx, orthopyroxene. Reference sample BCR-2g was analyzed as unknown together with the samples.

probably due to percolation of enriched fluids or fluid-rich, small-fraction melts. It is possible that reaction with the same fluids formed spongy domains with silicate inclusions and vesicles in spinel (Ionov et al., 2011).

(3) Shortly before the transport of the xenoliths to the surface, parental magmas of Bezymianny volcano intruded their source regions along fractures, then fragmented their host mantle rocks and carried them upwards (first to intermediate chambers, then to the surface). The fragmented mantle rocks were heated, fractured and invaded by fluids and liquids emanating from the magmas. In addition to forming the Fe-rich rims of the xenoliths, these processes formed crosscutting veins and deposited interstitial 3rd-generation materials in the xenoliths. These materials are usually enriched in magma-related components (Fe, Al, Ca, alkalis) and also show broad compositional ranges (Fig. 4) because they are products of localized, multi-stage, often disequilibrium peridotite–melt reaction products.

The Bezymianny xenoliths show similarities in terms of modal and major element compositions to the majority of arc mantle peridotites from the western Pacific exposed on the ocean floor or found as xenoliths, i.e. most of them are harzburgitic residues of high-degree partial melting (e.g. Parkinson and Pearce, 1998; Bryant et al., 2007; Ishimaru et al., 2007; Ionov, 2010). Another feature that the Bezymianny xenoliths share with the other mantle peridotites from the western Pacific is high oxygen fugacity, which is commonly attributed either to melting triggered by oxidized, slab-derived, water-rich fluids or to post-melting metasomatism induced by such fluids (see Section 4).

By comparison, the mineralogical and chemical compositions of metasomatic products or their abundances in the rocks are locally different in the western Pacific occurrences. Typical for many of them is the widespread development of fine-grained (often fibrous), opx-rich aggregates replacing either primary olivine (McInnes et al., 2001; Bryant et al., 2007; Ishimaru et al., 2007) or coarse-grained opx (Ionov, 2010) usually attributed to late-stage metasomatism by slab-derived, silica-rich fluids. Orthopyroxene in the Bezymianny xenoliths predominantly occurs as coarse grains (Figs. 2a and 3a) and does not normally replace olivine, by contrast to fibrous opx in xenoliths from nearby Shiveluch (Bryant et al., 2007). Fine-grained opx-rich aggregates are rare and only present at xenolith rims (Fig. 2a–b), late-stage veins and recrystallization zones due to heating by host magmas (Fig. 2c).

Published data on trace elements in arc mantle xenoliths are rare, in particular for opx. Important data suites have been reported for xenoliths from the Batan Island in the Philippines (Schiano et al., 1995) and seamounts off the coast of Papua-New Guinea (Grégoire et al., 2001; McInnes et al., 2001) as well as for serpentinized peridotites dredged in the Izu–Bonin–Mariana forearc (Parkinson and Pearce, 1998). Compared to the peridotites from Bezymianny, the Batan and some Papua-New Guinea xenoliths are more metasomatized (or reacted with host magmas), i.e. contain veins and accessory mica as

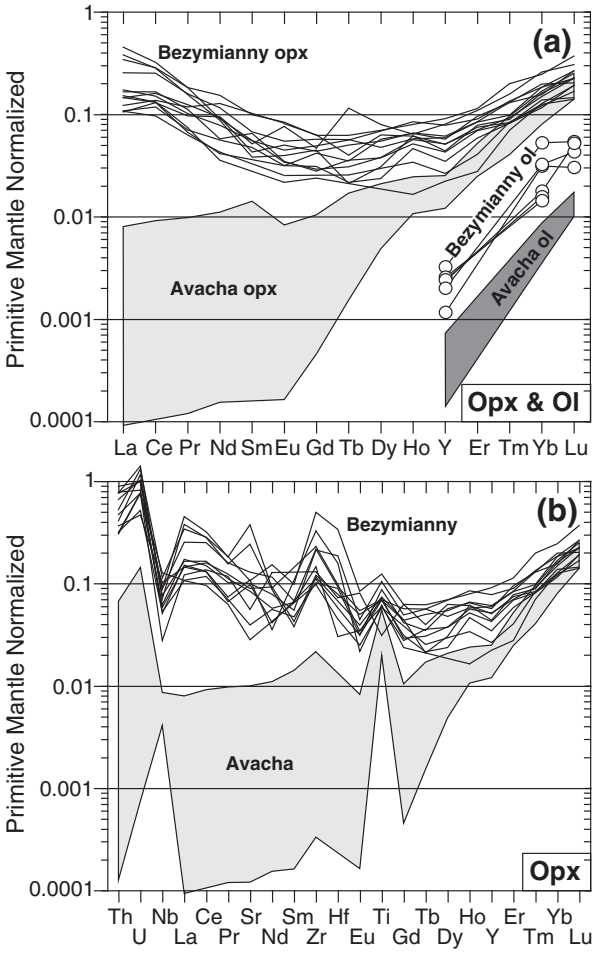

Fig. 5. a–b. Primitive mantle-normalized (McDonough and Sun, 1995) trace element patterns for coarse opx and olivine from xenolith CK09-7c: (a) rare earth elements (REE) and Y, (b) extended trace element patterns. Also shown are composition fields (filled in gray) for opx and olivine in Avacha xenoliths (Ionov, 2010).

well as more abundant amph and have high whole-rock abundances of alkalis, Ti and incompatible trace elements (Vidal et al., 1989; Maury et al., 1992; Grégoire et al., 2001). Hence, the SW Pacific xenoliths may have been more affected by late-stage melt/fluid circulation in the mantle, likely related to the magmas that carried the xenoliths to the surface, than those from Bezymianny.

7. Along-arc variations of mantle compositions in Kamchatka

Peridotite xenoliths of certain mantle origin have been reported in international peer-reviewed literature for only two volcanoes on the EVF in Kamchatka: Avacha (320 km south of Bezymianny) and Shiveluch (86 km north of Bezymianny, Fig. 1). The Bezymianny xenoliths in this study are generally similar in microstructures, modal and major element compositions (Fig. 4) to harzburgite xenoliths reported from Avacha (Ishimaru et al., 2007; Ionov, 2010), except that some Avacha xenoliths contain opx with fine-grained rims. The most important difference, as shown in this paper, is greater enrichments in incompatible trace elements in coarse opx from the Bezymianny harzburgites (Fig. 5), which indicate higher degrees of cryptic metasomatism that took place in the lithospheric mantle beneath Bezymianny well before the transport of the xenoliths to the surface.

Petrographic and major element data were recently reported for 26 xenoliths from Shiveluch (Bryant et al., 2007). These xenoliths are predominantly coarse to porphyroclastic spinel harzburgites with subordinate dunites, lherzolites and various pyroxenites. Importantly, opx in the Shiveluch peridotites is fine-grained, usually fibrous, and is attributed to late-stage replacement of olivine (Bryant et al., 2007). By contrast, as discussed in Section 6, opx in the Bezymianny xenoliths is coarse and appears to be residual after melt extraction. Furthermore, the compositions of olivine and pyroxenes in the Shiveluch harzburgites differ from those in the Bezymianny xenoliths (Fig. 4). Bryant et al. (2007) proposed a complex, multi-stage sequence of events to explain the origin of the Shiveluch harzburgites: (1) melt extraction formed harzburgites, (2) melt percolation replaced opx by olivine and converted harzburgites to dunites, (3) late-stage percolation of silica-rich hydrous fluids/melts replaced some olivine in the majority of dunites by fine-grained opx, (4) percolation of final-stage, volatile-rich products formed veins of amph–phlogopite–opx. If this is correct, the Bezymianny xenoliths experienced a different post-melting evolution because they show no significant evidence for stages b–d (even though definitive conclusions may require studies of more samples). Alternatively, fine-grained opx in the mantle beneath Shiveluch may have formed mainly by replacement of coarse opx rather than of olivine as recently suggested for xenoliths from Avacha (Ionov, 2010). In the latter case, stage (b) is not necessary to form harzburgites and there may be more similarities in post-melting history with the Bezymianny suite.

Ultramafic xenoliths dominated by pyroxenites, but also including harzburgites, occur at Kharchinsky volcano 20 km south of Shiveluch (Bryant et al., 2007), but no specific data on those xenoliths have been published in peer-reviewed literature. Preliminary data (Mobley et al., 2008) indicate higher 2-pyroxene equilibration T estimates for the Kharchinsky peridotites (1000–1050 °C) compared to peridotites from Shiveluch and Avacha, which may be due to a higher heat flux through the lithospheric mantle.

To sum up, our results suggest that the mantle beneath the modern Kamchatka arc was initially formed as refractory harzburgitic residues of high-degree melt extraction, most likely by hydrous melting in subduction settings. These residues experienced metasomatism due to percolation of fluids and small-fraction, fluid-rich melts, which was more active in the mantle beneath the northern Kamchatka (Bezymianny), notably with greater enrichments of opx in incompatible trace elements. Furthermore, the lithospheric mantle in the northernmost segment of the Kamchatka arc (beneath Shiveluch and Kharchinsky) shows evidence for widespread reaction of wall-rock peridotites with percolating high-T melts at high melt/rock ratios and formation of cumulates. We attribute stronger metasomatism and melt flux to the arc structure in that region, e.g. a location above or close to a slab boundary or slab anomaly, possibly with lateral asthenospheric mantle flow around the edge of the Pacific plate (Peyton et al., 2001; Yogodzinski et al., 2001; Levin et al., 2002; Davaille and Lees, 2004; Jiang et al., 2009), which supplies more heat and fluids and causes higher magma production.

8. Conclusions

(1) Peridotite xenoliths from Bezymianny volcano are coarse to porphyroclastic spinel harzburgites consisting predominantly of coarse- to medium-grained olivine and opx, with subordinate late-stage, fine-grained interstitial or vein materials made up of pyroxenes, spinel, amphibole and feldspar.
(2) The lithospheric arc mantle beneath Bezymianny was initially formed by high-degree (≥30%) melt extraction, likely by hydrous melting in subduction settings, to produce refractory cpx-free, low-opx harzburgitic residues. The residues subsequently cooled down to 800–900 °C and were enriched in incompatible trace elements by cryptic metasomatism as suggested by spoon-shaped patterns of coarse opx.
(3) Comparisons of the data on the Bezymianny xenoliths with those from Avacha and Shiveluch suggest significant along-arc compositional variations in the lithospheric mantle. First, the mantle beneath Bezymianny, and possibly the Klyucheskoy Group volcanoes in general, appears to have experienced greater cryptic

metasomatism by fluids or small-fraction melts, indicated by higher abundances of incompatible trace elements in coarse opx compared to those in xenoliths from Avacha in southern Kamchatka. Second, the lithospheric mantle north of the Klyucheskoy Group appears to contain more cumulates and hybrid rocks produced by reaction of residual peridotites with percolating melts at high melt/rock ratios.

(4) The along-arc variations in the composition of the lithospheric mantle beneath Kamchatka, and possibly elsewhere, appear to be related to arc structure. The metasomatism and melt–rock reactions, hence overall upward fluid and melt flux, may be stronger near slab boundaries or slab anomalies and may be linked, in particular, to asthenospheric mantle flow around plate edges, which causes higher magma production and fluid flux.

Supplementary data to this article can be found online at http://dx.doi.org/10.1016/j.jvolgeores.2012.12.022.

Acknowledgments

We thank the PIRE-Kamchatka team for the assistance in fieldwork and V.O. Yapaskurt and J.L. Devidal for analytical and technical assistance. DAI acknowledges a PNP grant from Institut National de Sciences de l'Univers (INSU-CNRS, France) in 2011 and PICS-CNRS grant no. 5812 for the collaboration with Russian Academy of Sciences in 2011–2013. Fieldwork was funded by the NSF PIRE — Kamchatka Award OISE 0530278. PYP and SVD appreciate the support from M.V. Lomonosov Moscow State University Program of Development and RFBR grant 12-05-00941-a.

References

Bedini, R.M., Bodinier, J.-L., 1999. Distribution of incompatible trace elements between the constituents of spinel peridotite xenoliths: ICP-MS data from the East African rift. Geochimica et Cosmochimica Acta 63 (22), 3883–3900.

Bénard, A., Ionov, D.A., 2012. A new petrogenetic model for low-Ca boninites: evidence from veined sub-arc xenoliths on melt–mantle interaction and melt fractionation. Geochemistry, Geophysics, Geosystems 13 (1), Q0AF05. http://dx.doi.org/10.1029/2012GC004145.

Bénard, A., Palle, S., Doucet, L.S., Ionov, D.A., 2011. Three-dimensional imaging of sulfides in silicate rocks at submicron resolution with multiphoton microscopy. Microscopy and Microanalysis 17 (06), 937–943.

Brandon, A.D., Draper, D.S., 1996. Constraints on the origin of the oxidation state of mantle overlying subduction zones: an example from Simcoe, Washington, USA. Geochimica et Cosmochimica Acta 60 (10), 1739–1749.

Brey, G.P., Köhler, T., 1990. Geothermobarometry in four-phase lherzolites II. New thermobarometers, and practical assessment of existing thermobarometers. Journal of Petrology 31, 1353–1378.

Bryant, J.A., Yogodzinski, G.M., Churikova, T.G., 2007. Melt–mantle interactions beneath the Kamchatka arc: evidence from ultramafic xenoliths from Shiveluch volcano. Geochemistry, Geophysics, Geosystems 8, Q04007. http://dx.doi.org/10.1029/2006GC001443.

Churikova, T., Wörner, G., Mironov, N., Kronz, A., 2007. Volatile (S, Cl and F) and fluid mobile trace element compositions in melt inclusions: implications for variable fluid sources across the Kamchatka arc. Contributions to Mineralogy and Petrology 154 (2), 217–239.

Davaille, A., Lees, J.M., 2004. Thermal modeling of subducted plates: tear and hotspot at the Kamchatka corner. Earth and Planetary Science Letters 226 (3–4), 293–304.

Dorendorf, F., Wiechert, U., Wörner, G., 2000. Hydrated sub-arc mantle: a source for the Klyuchevskoy volcano, Kamchatka/Russia. Earth and Planetary Science Letters 175, 69–86.

Eichelberger, J., Gordeev, E., Kasahara, M., Izbekov, P., Lees, J., 2007. Volcanism and Subduction: The Kamchatka region. Amer. Geophys. Union, Washington, DC (369 pp.).

Gorbatov, A., Dominguez, J., Suarez, G., Kostoglodov, V., Zhao, D., Gordeev, E., 1999. Tomographic imaging of the P-wave velocity structure beneath the Kamchatka peninsula. Geophysical Journal International 137 (2), 269–279.

Grégoire, M., McInnes, B.I.A., O'Reilly, S.Y., 2001. Hydrous metasomatism of oceanic sub-arc mantle, Lihir, Papua New Guinea — part 2. Trace element characteristics of slab-derived fluids. Lithos 59 (3), 91–108.

Halama, R., Savov, I., Rudnick, R., McDonough, W., 2009. Insights into Li and Li isotope cycling and sub-arc metasomatism from veined mantle xenoliths, Kamchatka. Contributions to Mineralogy and Petrology 158 (2), 197–222.

Herzberg, C., 2004. Geodynamic information in peridotite petrology. Journal of Petrology 45 (12), 2507–2530.

Hopp, J., Ionov, D.A., 2011. Tracing partial melting and subduction-related metasomatism in the Kamchatkan mantle wedge using noble gas compositions. Earth and Planetary Science Letters 302 (1–2), 121–131.

Ionov, D.A., 2010. Petrology of mantle wedge lithosphere: new data on supra-subduction zone peridotite xenoliths from the andesitic Avacha volcano, Kamchatka. Journal of Petrology 51 (1–2), 327–361.

Ionov, D.A., Seitz, H.M., 2008. Lithium abundances and isotopic compositions in mantle xenoliths from subduction and intra-plate settings: mantle sources versus eruption histories. Earth and Planetary Science Letters 266 (3–4), 316–331.

Ionov, D.A., Wood, B.J., 1992. The oxidation state of subcontinental mantle: oxygen thermobarometry of mantle xenoliths from central Asia. Contributions to Mineralogy and Petrology 111, 179–193.

Ionov, D.A., O'Reilly, S.Y., Griffin, W.L., 1997. Volatile-bearing minerals and lithophile trace elements in the upper mantle. Chemical Geology 141, 153–184.

Ionov, D.A., Grégoire, M., Prikhod'ko, V.S., 1999. Feldspar–Ti-oxide metasomatism in off-cratonic continental and oceanic upper mantle. Earth and Planetary Science Letters 165 (1), 37–44.

Ionov, D.A., Ashchepkov, I., Jagoutz, E., 2005a. The provenance of fertile off-craton lithospheric mantle: Sr–Nd isotope and chemical composition of garnet and spinel peridotite xenoliths from Vitim, Siberia. Chemical Geology 217 (1–2), 41–75.

Ionov, D.A., Chanefo, I., Bodinier, J.-L., 2005b. Origin of Fe-rich lherzolites and wehrlites from Tok, SE Siberia by reactive melt percolation in refractory mantle peridotites. Contributions to Mineralogy and Petrology 150 (3), 335–353.

Ionov, D., Bénard, A., Plechov, P., 2011. Melt evolution in subarc mantle: evidence from heating experiments on spinel-hosted melt inclusions in peridotite xenoliths from the andesitic Avacha volcano (Kamchatka, Russia). Contributions to Mineralogy and Petrology 162 (6), 1159–1174.

Ishimaru, S., Arai, S., 2011. Peculiar Mg–Ca–Si metasomatism along a shear zone within the mantle wedge: inference from fine-grained xenoliths from Avacha volcano, Kamchatka. Contributions to Mineralogy and Petrology 161 (5), 703–720.

Ishimaru, S., Arai, S., Ishida, Y., Shirasaka, M., Okrugin, V.M., 2007. Melting and multistage metasomatism in the mantle wedge beneath a frontal arc inferred from highly depleted peridotite xenoliths from the Avacha volcano, southern Kamchatka. Journal of Petrology 48 (2), 395–433.

Jiang, G., Zhao, D., Zhang, G., 2009. Seismic tomography of the Pacific slab edge under Kamchatka. Tectonophysics 465 (1–4), 190–203.

Kelemen, P.B., Dick, H.J., Quick, J.E., 1992. Formation of harzburgite by pervasive melt/rock reaction in the upper mantle. Nature 358, 635–641.

Konstantinovskaya, E.A., 2001. Arc–continent collision and subduction reversal in the Cenozoic evolution of the Northwest Pacific: an example from Kamchatka (NE Russia). Tectonophysics 333, 75–94.

Koulakov, I., Gordeev, E.I., Dobretsov, N.L., Vernikovsky, V.A., Senyukov, S., Jakovlev, A., 2011. Feeding volcanoes of the Kluchevskoy group from the results of local earthquake tomography. Geophysical Research Letters 38 (9), L09305. http://dx.doi.org/10.1029/2011GL046957.

Levin, V., Shapiro, N., Park, J., Ritzwoller, M., 2002. Seismic evidence for catastrophic slab loss beneath Kamchatka. Nature 418 (6899), 763–767.

Manea, V.C., Manea, M., Kostoglodov, V., Sewell, G., 2005. Thermal models, magma transport and velocity anomaly estimation beneath southern Kamchatka. In: Foulger, G.R., Natland, J.H., Presnall, D.C., Anderson, D.L. (Eds.), Plates, Plumes, and Paradigms: Geol. Soc. Amer. Spec. Paper 388. GCA, Boulder, pp. 517–536.

Maury, R.C., Defant, M.J., Joron, J.-L., 1992. Metasomatism of the sub-arc mantle inferred from trace elements in Philippine xenoliths. Nature 360, 661–663.

McDonough, W.F., Sun, S.-s., 1995. The composition of the Earth. Chemical Geology 120, 223–253.

McInnes, B.I.A., Gregoire, M., Binns, R.A., Herzig, P.M., Hannington, M.D., 2001. Hydrous metasomatism of oceanic sub-arc mantle, Lihir, Papua New Guinea: petrology and geochemistry of fluid-metasomatised mantle wedge xenoliths. Earth and Planetary Science Letters 188 (1–2), 169–183.

Mobley, R., Dektor, C., Yogodzinski, G., Churikova, T., 2008. Mineralogy and petrology of ultramafic xenoliths from Kharchinsky Volcano, Kamchatka. 2008 Meeting of the Geological Society of America, Abstract No. 193–118.

Nikulin, A., Levin, V., Shuler, A., West, M., 2010. Anomalous seismic structure beneath the Klyuchevskoy Group, Kamchatka. Geophysical Research Letters 37 (14), L14311. http://dx.doi.org/10.1029/2010GL043904.

Parkinson, I.J., Arculus, R.J., 1999. The redox state of subduction zones: insights from arc-peridotites. Chemical Geology 160 (4), 409–423.

Parkinson, I.J., Pearce, J.A., 1998. Peridotites from the Izu–Bonin–Mariana forearc (ODP Leg 125): evidence for mantle melting and melt–mantle interaction in a supra-subduction zone setting. Journal of Petrology 39 (9), 1577–1618.

Parkinson, I.J., Arculus, R.J., Eggins, S.M., 2003. Peridotite xenoliths from Grenada, Lesser Antilles Island Arc. Contributions to Mineralogy and Petrology 146 (2), 241–262.

Pearson, D.G., Canil, D., Shirey, S.B., 2003. Mantle samples included in volcanic rocks: xenoliths and diamonds. In: Carlson, R.W. (Ed.), Treatise on Geochemistry. The Mantle and Core, Vol. 2. Elsevier, pp. 171–276.

Peyton, V., Levin, V., Park, J., Brandon, M., Lees, J., Gordeev, E., Ozerov, A., 2001. Mantle flow at a slab edge: seismic anisotropy in the Kamchatka region. Geophysical Research Letters 28 (2), 379–383.

Piip, B.I., 1956. Klyuchevshoy volcano and its eruptions in 1944–1945 and during the past years. Proc. Lab. Volcanol., 11, pp. 1–309 (in Russian).

Pogge von Strandmann, P.A.E., Elliott, T., Marschall, H.R., Coath, C., Lai, Y.-J., Jeffcoate, A., Ionov, D.A., 2011. Variations of Li and Mg isotope ratios in bulk chondrites and mantle xenoliths. Geochimica et Cosmochimica Acta 75 (18), 5247–5268.

Portnyagin, M., Hoernle, K., Plechov, P., Mironov, N., Khubunaya, S., 2007. Constraints on mantle melting and composition and nature of slab components in volcanic arcs from volatiles (H_2O, S, Cl, F) and trace elements in melt inclusions from the Kamchatka Arc. Earth and Planetary Science Letters 255 (1–2), 53–69.

Schiano, P., Clocchiatti, R., Shimizu, N., Maury, R.C., Jochum, K.P., Hofman, A.W., 1995. Hydrous, silica-rich melts in the sub-arc mantle and their relationships with erupted arc lavas. Nature 377, 595–600.

Shcherbakov, V.D., Plechov, P.Y., 2010. Petrology of mantle xenoliths in rocks of the Bezymiannyi Volcano (Kamchatka). Doklady Earth Sciences 434 (2), 782–785.

Shcherbakov, V., Plechov, P., Izbekov, P., Shipman, J., 2011. Plagioclase zoning as an indicator of magma processes at Bezymianny Volcano, Kamchatka. Contributions to Mineralogy and Petrology 162 (1), 83–99.

Soustelle, V., Tommasi, A., Demouchy, S., Ionov, D.A., 2010. Deformation and fluid–rock interaction in the supra-subduction mantle: microstructures and water contents in peridotite xenoliths from the Avacha volcano, Kamchatka. Journal of Petrology 51 (1–2), 363–394.

Turner, S., Sims, K.W.W., Reagan, M., Cook, C., 2007. A ^{210}Pb–^{226}Ra–^{230}Th–^{238}U study of Klyuchevskoy and Bezymianny volcanoes, Kamchatka. Geochimica et Cosmochimica Acta 71 (19), 4771–4785.

Tursack, E., Liang, Y., 2012. A comparative study of melt–rock reactions in the mantle: laboratory dissolution experiments and geological field observations. Contributions to Mineralogy and Petrology 163 (5), 861–876.

van Keken, P.E., 2003. The structure and dynamics of the mantle wedge. Earth and Planetary Science Letters 215 (3–4), 323–338.

Vidal, P., Dupuy, C., Maury, R., Richard, M., 1989. Mantle metasomatism above subduction zones: trace-element and radiogenic isotope characteristics of peridotite xenoliths from Batan Island (Philippines). Geology 17, 1115–1118.

Walter, M.J., 2003. Melt extraction and compositional variability in mantle lithosphere. In: Carlson, R.W. (Ed.), Treatise on Geochemistry. The Mantle and Core, Vol. 2. Elsevier, Amsterdam, pp. 363–394.

Weyer, S., Ionov, D.A., 2007. Partial melting and melt percolation in the mantle: the message from Fe isotopes. Earth and Planetary Science Letters 259 (1–2), 119–133.

Wood, B.J., Bryndzya, L.T., Johnson, K.E., 1990. Mantle oxidation state and its relationship to tectonic environment and fluid speciation. Science 248, 337–344.

Yogodzinski, G.M., Lees, J.M., Churikova, T.G., Dorendorf, F., Woerner, G., Volynets, O.N., 2001. Geochemical evidence for the melting of subducting oceanic lithosphere at plate edges. Nature 409 (6819), 500–504.